Monitoring Welding Torch Position and Posture Using Reversed Electrode Images – Part II, Experimental and Analysis for the REI-TPA Model

A new method was developed to relate welding torch position and attitude to reversed electrode images on the weld pool surface during GTAW

BY Y. FU, Q. LIU, R. XIAO, AND S. B. CHEN

Abstract

This paper is a sequel to the previous paper. In the previous research (Ref. 1), a REI-TPA model was established to quantitively relate reversed electrode images (REIs) to welding torch position and attitude (TPA). In this research, the REI-TPA model was validated with bead-on-plate welding experiments on S304 stainless steel plates. The contours of the REI and electrode as well as the weld pool geometry were extracted from the image with a developed, robust algorithm, and the arc length was calculated with welding voltage. The offset distance and deflection angle of the welding torch relative to the correct position and attitude were calculated by inputting the extracted parameters into the REI-TPA model. The computational result was compared to the experimental data. The result showed that the model is correct and the monitoring of the welding torch with the REI-TPA model is available. The REI-TPA model can be applied to real-time control of TPA, which is a supplement to the application of the weld passive visual image and an extension of multi-information acquisition and processing methods in the welding process.

Keywords

- Passive Vision
- Reversed Electrode Image
- Position and Attitude of Welding Torch

Introduction

In the previous paper (Ref. 1), the REI-TPA model was established to quantitively calculate welding torch position and attitude with the feature of REIs (reversed electrode images). This paper is a sequel to the previous paper and focuses on the adaptive extraction of the required parameters and the experimental validation of the REI-TPA model.

Sensing, modeling, and control are the key technologies of intelligent welding manufacturing (Refs. 2–4). The position and attitude of the welding torch (TPA) relative to the weld seam is of vital importance to the realization of intelligent welding manufacturing (Ref. 5) and are the basis of arc welding robot control and offline programming, directly affecting the quality of the produced weld. With the REI-TPA model, TPA can be calculated with the feature of REIs (Refs. 6–9). Active and passive vision sensing techniques may be used to collect REIs and other visual information needed during the welding process.

In passive vision sensing systems (Refs. 10–14], the arc light functions as the light source for the camera, and the experimental setup is simple and easy to operate. Wu et al. (Ref. 14) developed a practical and efficient weld pool edge extraction software based on a passive vision system for GTAW. 2D information of the weld pool was extracted from the images, and the Hammerstein model was then established to control the weld penetration state. Chen et al. (Refs. 12, 13) designed a double-sided sensing system capable of imaging the topside and backside of the weld pool. Bead-on-plate welding and butt joint welding were performed to establish the backside width predicting model with this sensing system, and an automatic welding control system was established with a proportional–integral–derivative (PID) controller and a fuzzy neural network. The work by Chen et al. (Refs. 12, 13) was a supplement to the collection, processing, and application of weld passive vision sensing.

https://doi.org/10.29391/2024.103.021

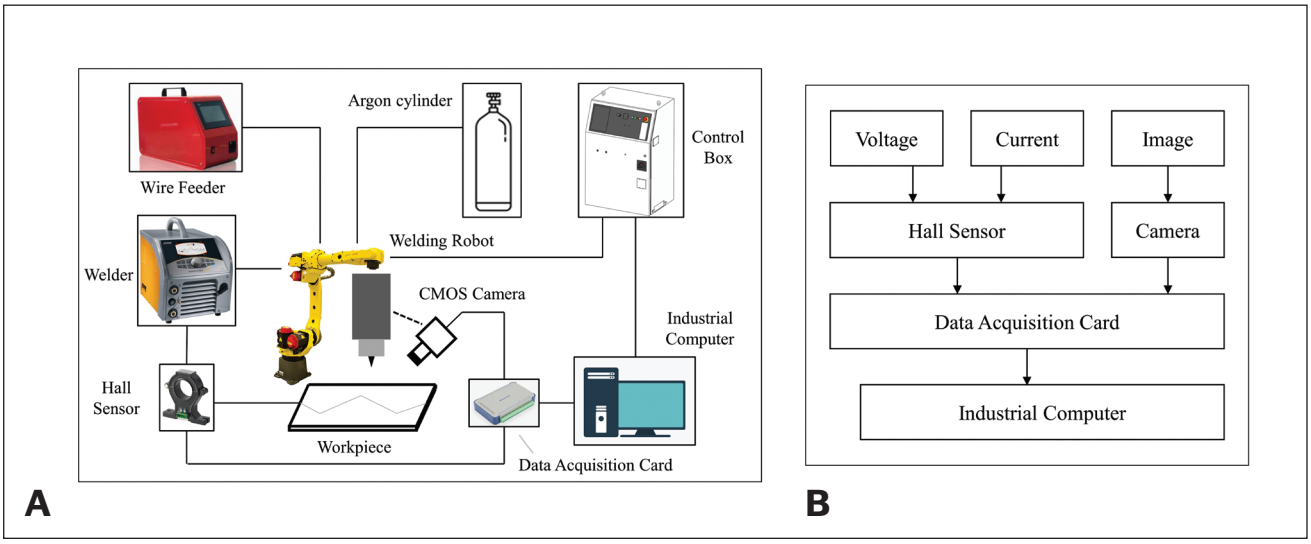

Fig. 1 — A — Schematic of the experimental system; B — The data collection process.

As for active vision sensing systems (Refs. 15–21), auxiliary laser light is applied to illuminate the weld pool area or part of the area. Thus, the interference of arc light is reduced, and the image processing is relatively simple. Zhang and Kovacevic et al. (Refs. 17–19) collected high-quality weld pool images with a high-speed shutter camera and pulsed laser light source during GTAW. The edges and geometrical appearance of the weld pool were extracted from the images, and an adaptive closed-loop control system was developed to control the welding process. Zhang and Song et al. (Refs. 20, 21) designed a set of weld pool visual inspection systems with a lattice laser transmitter. The laser emitted lattice-structured light, and the light was distorted after being reflected by the weld pool and irradiated on the projection plate and then collected by the camera. Based on the obtained images, an interpolation reconstruction scheme (IRS) and extrapolation reconstruction scheme (ERS) were used to reconstruct the 3D surface of the weld pool. Zhang et al. have made great contributions to the field of active welding vision sensing, providing feasible methods for relatively accurate measurement and reconstruction of 3D weld pool surfaces.

At present, the main method of monitoring the position and attitude of the welding torch is to use various sensors, although these methods all have certain limitations. In the previous investigation (Ref. 1), the REI-TPA model was established to monitor TPA in real-time. With the model, only a camera and Hall sensor are needed, and the image acquisition is based on passive vision sensing, the experimental setup is low cost, and the data collection process is simple.

The main work from this research is the experimental and computational validation of the REI-TPA model, including the collection and extraction of the needed parameters, and the auto-calculation of the TPA. The calculation and verification of the REI-TPA model were conducted offline based on bead-on-plate GTAW using an S304 stainless steel plate. A robust algorithm was developed to automatically extract the REI and other required features from the passive visual image of the weld pool. The position and attitude of the welding torch calculated with the REI-TPA model were compared with the preset experimental data. The result showed that the model is correct and monitoring of the welding torch with the REI-TPA model is feasible.

The novel introduction of the REI-TPA model is an attempt to relate weld passive vision images to TPA, which contributes to automated welding and weld quality control. The model can be applied to real-time monitoring and correction of TPA after further research and improvement of equipment accuracy.

Experimental Setup and Welding Parameters

Experimental Setup

The diagram of the experimental system is shown in Fig. 1A. GTAW was performed using a FANUC arc welding robot; the robot can move according to preset position and attitude. The pose information of the tool center point (TCP) in the world coordinate system can be obtained from the teaching pendant in real time. Before the welding experiment, the tool coordinate system of the welding torch was determined with the "six points teaching" method, and the TCP was set at the tip of the electrode.

The welding data collection process is shown in Fig. 1B. During the welding process, the image of the weld pool, welding current, and voltage were collected with the Xiris XVC-1000/1100 CMOS welding camera and Hall sensor, respectively. The camera was fixed on the welding torch with an appropriate angle so that the electrode, weld pool, and REI could be collected clearly at the same time. A dimming film was set before the lens of the camera to filter out redundant arc light. The aperture was set at f.22 to reduce the amount of light reaching the image sensor. The resolution of the camera was 1280 × 1024 pixels, and the size of the CMOS sensor was 8.7 × 7 mm; thus, the size of each pixel was 6.8 × 6.8 μm. The sampling frequency of the camera was 25 Hz, and the exposure time was 20 ms. The dynamic range of the image captured by the camera was more than

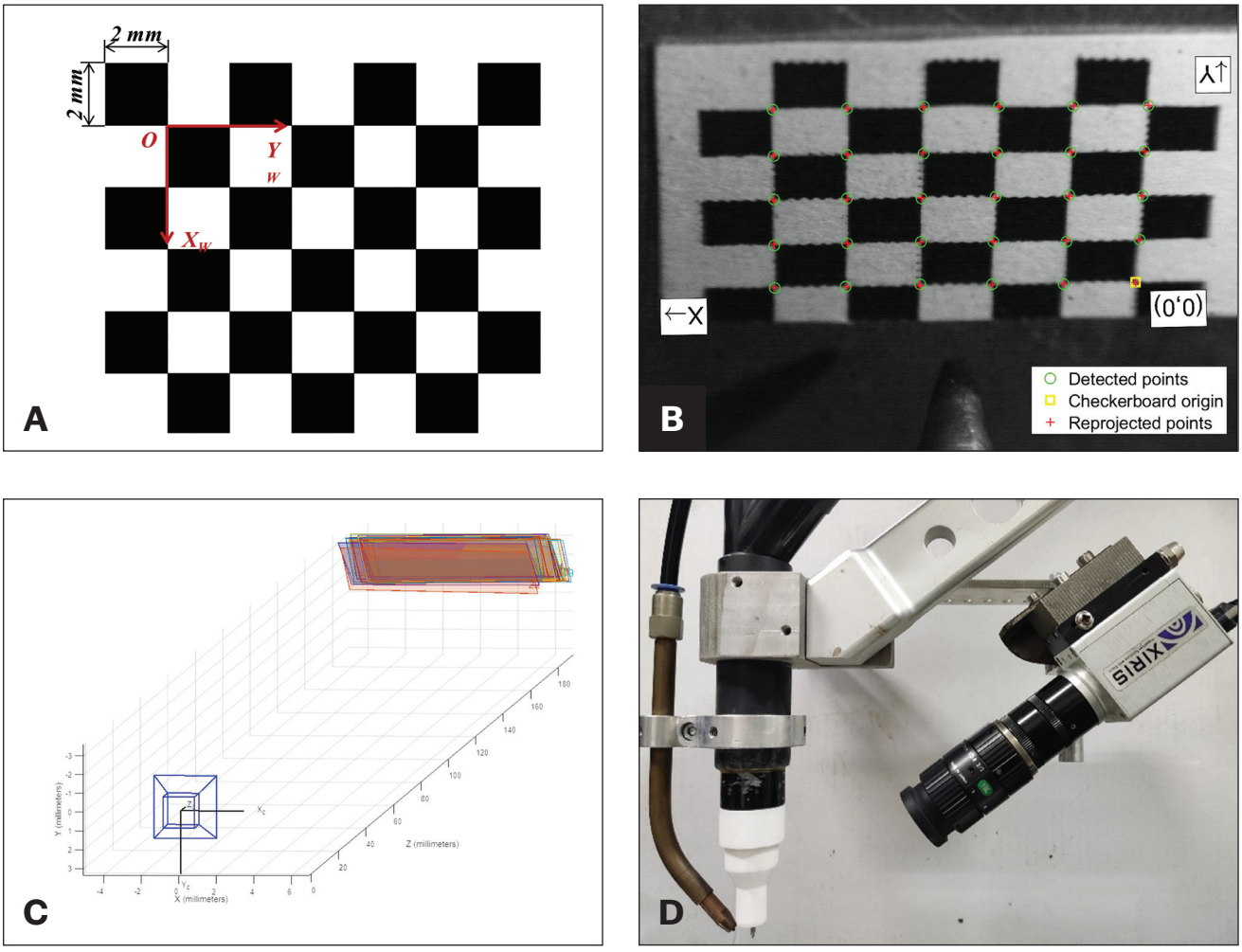

Fig. 2 — A — Relative position and attitude of the camera and welding torch; B — Shape and size of the calibration pattern; C — The relative position and attitude of the camera and calibration plate. D — Calibration pattern collected by the camera.

140 dB so that the bright foreground and the surrounding dark background could be observed clearly at the same time.

Experimental Materials and Experimental Parameters

The GTA welding experiment was implemented on an S304 stainless steel plate with a size of 200 × 60 × 3 mm. Before the welding experiments, the workpiece was polished and fixed on the work plate with fixtures. The tip of the tungsten electrode was ground to approximately 40 deg.

During GTAW, direct current with values of 100 A and 120 A was applied; under this level of current, the weld pool is stable. The workpiece and tungsten electrode were connected to the anode and cathode of the welding machine, respectively. In this case, the generated weld pool was deep and narrow, the deformation of the workpiece was small, and less heat was generated in the electrode.

To validate the REI-TPA model, five rounds of bead-on-plate welding experiments with various positions and attitudes of TCS were carried out. The parameters of each experiment are listed in the section "Welding Process."

Experimental Process

Camera Calibration

The position and attitude of the camera and welding torch are shown in Fig. 2A. Before the welding experiments, the focus length and pose of the camera relative to the welding torch were adjusted appropriately so that the electrode and REI could be captured clearly at the same time. Camera calibration was then performed to determine the parameters (S, f, θ). In this research, Zhang's calibration method was employed because of its high precision and robustness (Ref. 22). The shape and size of the calibration pattern are shown in Fig. 2B. A total of 50 calibration pattern images with different poses of calibration plates relative to the camera were collected, and 27 clear images were selected for calibration calculation. The relative pose of the camera and calibration plate of these 27

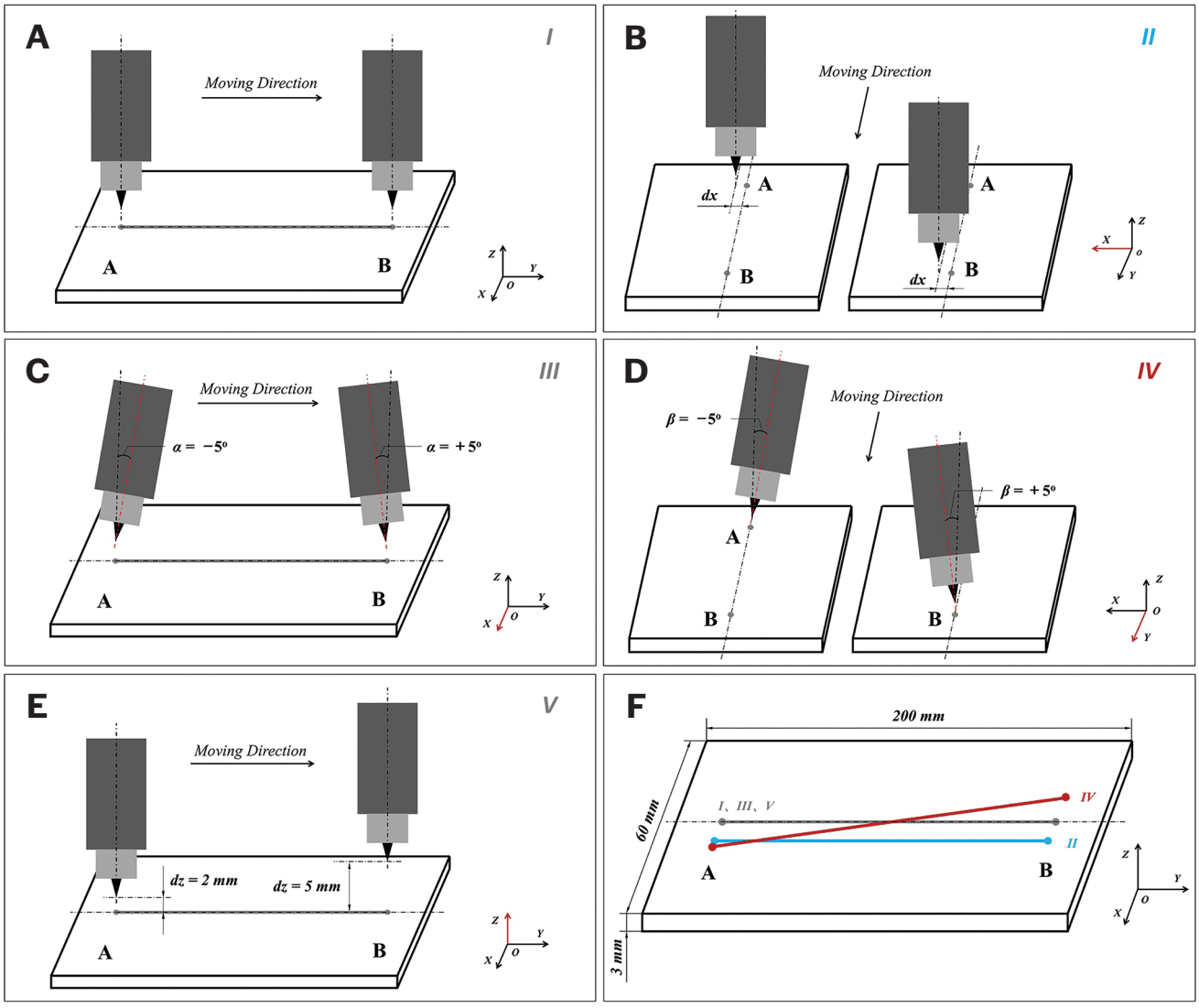

Fig. 3 — Position and attitude of welding torch relative to the workpiece at welding starting and ending point in each experiment: A — Experiment I; B — Experiment II; C — Experiment III; D — Experiment IV; E — Experiment V; F — The moving trajectory of electrode tip in each experiment.

Table 1 — Intrinsic and External Parameters of Camera

Focus length *f*	Object distance *S*	Setup angle θ
~59 mm	~178 mm	~70 deg

images is shown in Fig. 2C. Among the pictures, one captured the position and attitude of when the calibration plate was the same as the workpiece's during the welding experiment. The detected corner points of this image are shown in Fig. 2D. The parameters (S, f, θ) were calculated according to Fig. 2D. The results are listed in Table 1. The average error of calibration was 1.69 pixels. The pose of the camera relative to the welding torch and the focal length would not be adjusted after camera calibration so that the parameters (S, f, θ) remained unchanged during the subsequent experiments.

Welding Process

To validate the REI-TPA model, a bead-on-plate welding experiment was conducted on an S304 stainless steel plate with GTAW. The spatial position and attitude of the welding torch relative to the weld seam during the experiment are shown in Figs. 3A–E. During the welding process, the welding torch moved from welding starting point A to welding ending point B with a preset position and attitude according to the REI-TPA model. The experiments are numbered (I, II, III, IV, V) respectively, and the moving trajectory of the electrode tip in each experiment is shown in Fig. 3F. For each experiment, the welding speed was 3 mm/s, and the standoff distance between the tip of the electrode and the surface of the workpiece was 3 mm. Passive visual images of the weld pool, welding current, and voltage were collected simultaneously in the experiments.

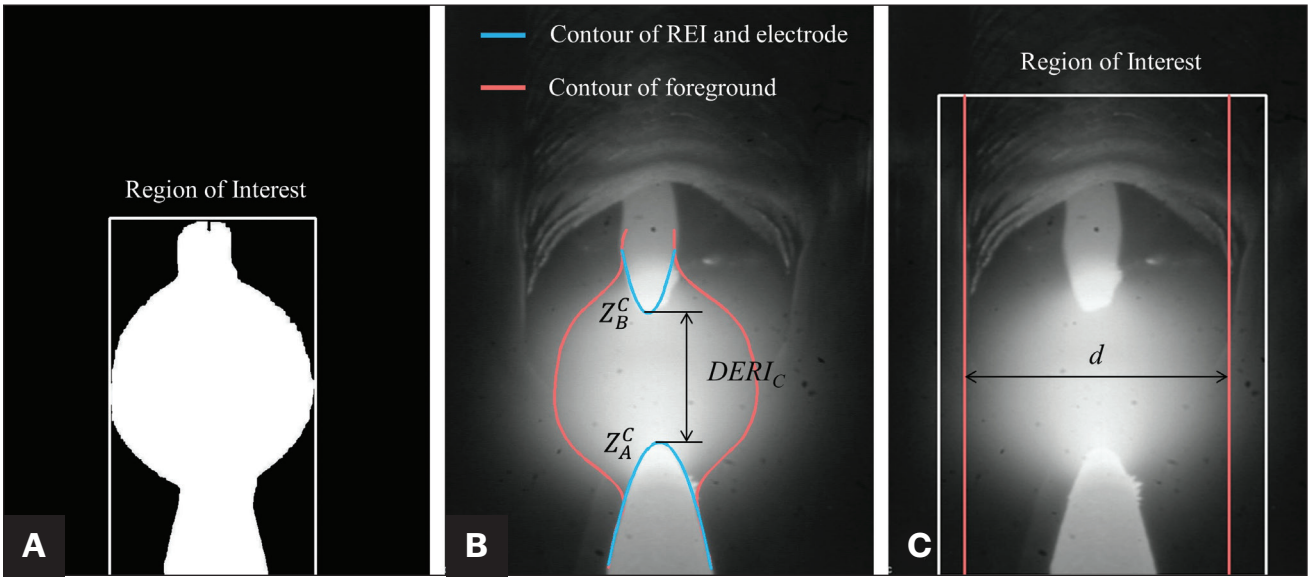

*Fig. 4 — A — Binary image obtained with a calculated threshold; B — Extracted contours of electrode and REI; C — Extracted width of weld pool. *Images here were cut to save space.*

In Experiments I, II, and V, the welding torch was perpendicular to the surface of the welding workpiece and remained unchanged during the welding process. In Experiment II, the welding torch deviated from the weld seam along the X-axis. In Experiment V, the standoff distance between the surface of the workpiece and the tip of the electrode increased from 2 mm at point A to 5 mm at point B during the welding process. In Experiments III and IV, the welding torch deflected around the X-axis and Y-axis from −5 deg to +5 deg relative to the weld pool coordinate system (WPCS), respectively, and the distance between the tip of the electrode and the surface of the workpiece remained unchanged. Specific parameters are shown in Table 2. To ensure the consistency of the experimental data, the welding parameters in experiments I–V were set to be the same.

Image Processing

According to Table 1, to calculate TPA, the geometric information of the weld pool and the position of the REIs relative to the electrode in the images of the weld pool were required. Hence, a robust algorithm was designed to automatically extract the contours of the electrode and REI and the width of the weld pool from the image of the weld pool. The flow chart of the algorithm is shown in Table 3 and Fig. 4.

In Ref. 23, the point with maximum intensity in the ROI window was selected as the tip of the REI. The algorithm was simple, quick, and convenient, while the extraction of ROI and tip point is easily affected by the arc light, which requires a high quality of the collected images. In this research, the binary threshold was calculated adaptively, and the arc light area was seen as a part of the foreground to be processed. Thus, the interference of arc light was eliminated. The algorithm can be applied to the processing of images with high-intensity spatter and arc light. With the developed

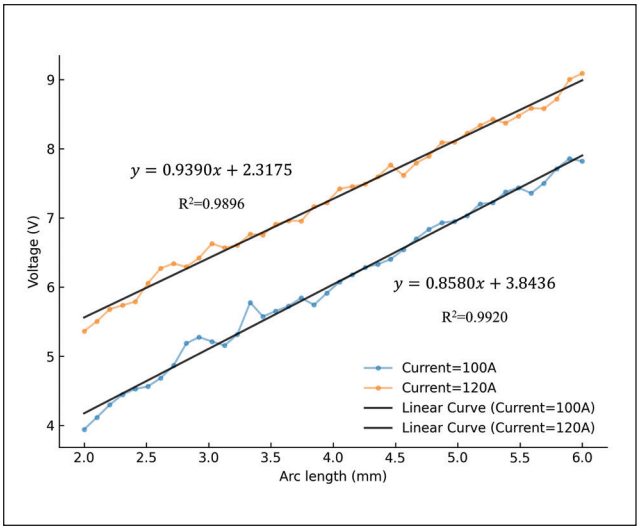

Fig. 5 — Linear relationship between welding voltage and arc length.

algorithm, parameters DERI ($DERI_C$, d, dy_C) can be calculated in real time with a maximum error of less than 0.15 mm.

Calculation of Arc Length

The object distance, u, in the imaging model of the weld pool surface equals the length of the welding arc. Much research has shown that when the welding current is determined, the arc length is proportional to the welding voltage (Refs. 24, 25). The linear relationship between arc length and welding voltage has been widely used in the arc length control system (Refs. 25, 27).

To establish the quantitative linear relationship between welding voltage and arc length, bead-on-plate welding exper-

Table 2 — Welding Parameters for Experiments I~V

Material	Thickness	Current	Travel Speed	Wire Feed Rate
S304	3 mm	120 A	3 mm/s	15 mm/s

Table 3 — Algorithm to Extract Contours of REI and Electrode, Width of Weld Pool from Image

Input: Image Sequence **Output: Coordinates of contour points of REI and electrode, $DERI_c$, d, dy_c**	
Extracting Contours of REI and Electrode	Calculating Width of Weld Pool
1. Image preprocessing, including image gray and median filtering.	1. Image preprocessing, including image gray and median filtering.
2. Calculating binary threshold adaptively with sliding window, then performing image binarization.	2. Calculating binary threshold adaptively according to pixel scale division, then performing image binarization.
3. Morphological processing and extracting region of interest.	3. Morphological processing and extracting region of interest.
4. Extracting coordinates of foreground contour points from binary image.	4. Determining the position of weld pool according to position of REI. Five lines with equal intervals inside weld pool area were selected.
5. Fitting contours with cubic B-spline curves.	5. Determining gray gradient curves of these five lines.
6. Smoothing the contour curves with Savitzky – Golay convolution method.	6. Determining left and right boundary of weld pool through the abrupt points at both ends of the gradient curve.
7. Dividing the contour curves to three parts (electrode curve, arc light curve, REI curve) according to the variation of curve gradient	7. Calculating d.
8. Fitting electrode and REI curves with quadratic function.	
9. Calculating $DERI_c$, dy_c.	

iments were conducted on S304 stainless steel plates. The thickness of the workpiece was 3 mm, and the current was set as 100 A and 120 A. During the welding process, no wire was fed. The standoff distance between the tip of the electrode and the surface of the workpiece was preset to increase from 2 mm at the starting point to 6 mm at the ending point. The welding voltage and current were collected with a Hall sensor in real time with a sampling frequency of 40,000 Hz. The distance between the tip of the electrode and the surface of the workpiece was approximately equal to the arc length since no wire was fed during welding.

The collected data of voltage were divided into 40 groups on average to reduce the interference of occasional noise that occurred in the voltage acquisition process. Then, the average value in each group of data was calculated, and 40 voltage points were obtained. Lastly, the squares method was applied to perform linear regression on the calculated voltage points; the obtained linear curves are shown in Fig. 5. Under 100 A and 120 A, the square R values of linear regression fitting were 0.9896 and 0.9920, and the average absolute errors were 0.0815 and 0.0748, respectively. The result indicated that the points were well in line with the regression curve.

With the linear relationship, arc length (i.e., object distance, *u*) can be calculated in real time during the welding process with welding voltage.

Results

In Experiment I, about 1000 images were collected, 70 images were selected at equal intervals, and three of the pictures are shown in Fig. 6A. The position of the electrode in the image remained unchanged because the camera was fixed on the welding torch. The weld pool, electrode, and REI were collected clearly in the image of the weld pool. $DERI_C$ and *d* were calculated for each of the 70 images with the designed algorithm. Accordingly, the collected data of voltage was divided into 70 groups, then the average value of voltage in each group was calculated. The arc length, *u*, was calculated with the obtained voltage in each group. Then *DERI* was calculated with the equation when welding with the torch in a normal pose in the REI-TPA model. After reducing the amplitude of noise, the curves of $DERI_C$, *d*, *u*, and *DERI* are shown in Figs. 7A–D. During the welding process, $DERI_C$ and *d* remained unchanged; *u* decreased slightly, leading to the slight reduction of *DERI* in the middle and later periods of the experiment. The average D value between the two *DERI* curves in Fig. 7D is about 0.143 mm.

In Experiment II, the obtained images were the same as in Experiment I, while the offset along the X-axis was difficult to calculate, which is discussed in the next section.

In Experiment III, about 1000 images were collected, and 70 of the images were selected at equal intervals; examples of the images are shown in Fig. 6B. As in Experiment I, $DERI_C$, *d*, and *u* were calculated for each of the selected 70 images; the obtained curves are shown in Figs. 8A–C. During the experiment, the welding torch rotated from –5 deg to +5 deg around the X-axis. Accordingly, $DERI_C$ decreased gradually, *u* decreased firstly then increased, and *d* remained the same. The calculated deflection angle around the X-axis is shown in Fig. 8D; the average error of the calculated deflection angle is about 1.15 deg.

In Experiment IV, about 900 images were collected and 75 of the images were selected at equal intervals; examples of the images are shown in Fig. 6C. REI in the images moved from the right side of the electrode to the left side gradually. Parameters dy_c, *d*, and *u* were calculated for each of the selected 75 images; the obtained curves are shown in Figs. 9A–C. During the experiment, the welding torch rotated from –5 deg to +5 deg around the Y-axis. Accordingly, dy_c increased from around –0.1 mm to 0.1 mm in the CMOS sensor, *u* decreased firstly then increased, and *d* remained unchanged. The calculated deflection angle around the Y-axis is shown in Fig. 9D; average error of the calculated deflection angle is about 2.31 deg.

In Experiment V, the welding current was set as 120 A, and the standoff distance between the tip of the electrode and the surface of the workpiece increased from 2 mm at the starting point to 5 mm at the ending point. The welding voltage was collected with a sampling frequency of 40,000 Hz. The data of voltage was separated into 50 groups, and 50 average voltage values were calculated. Then *u* was calculated with the linear relationship shown in Fig. 5. The calculated voltage and corresponding arc length are shown in Fig. 10.

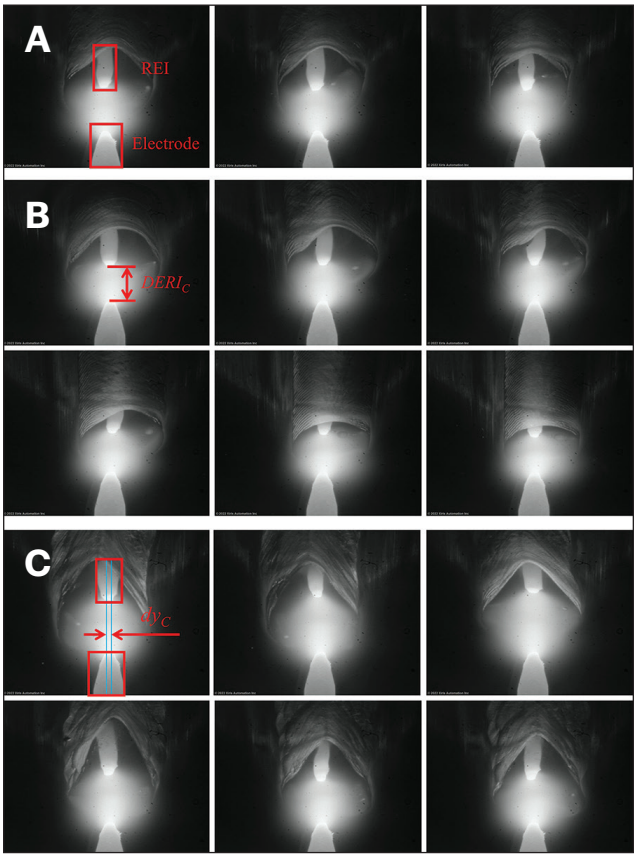

Fig. 6 — Images collected in each experiment: A — Experiment I; B — Experiment III; C — Experiment IV.

Discussion

Discussion of Experimental Results

By considering the weld pool surface as a spherical mirror, the REI-TPA model was established based on the feature of REIs extracted from passive vision images of the weld pool, and the experiment and calculation result implies that the model is valid and relatively accurate.

In Experiment I, *DERI* was calculated with two methods, and the difference between the two *DERI* curves was quite small, which suggests the imaging model of the weld pool surface is correct and the result of camera calibration is accurate.

In Experiment II, the offset distance along the X-axis was not calculated. To collect clear REI and electrodes, the camera focused on the weld pool area. Thus, the weld seam cannot be captured due to the block of the electrode, and the offset distance along the X-axis cannot be calculated. The position and profile of the weld seam can be obtained using a passive vision system with an additional camera focusing on the weld seam (Refs. 10, 28) as well as an active vision system with structure laser light (Refs. 26, 29).

In Experiments III and IV, as shown in Figs. 8D and 9D, fluctuation occurred in the curves of the calculated deflection angle due to the amplification effect of arc sine and arc tangent functions and the cumulation of the error in each required

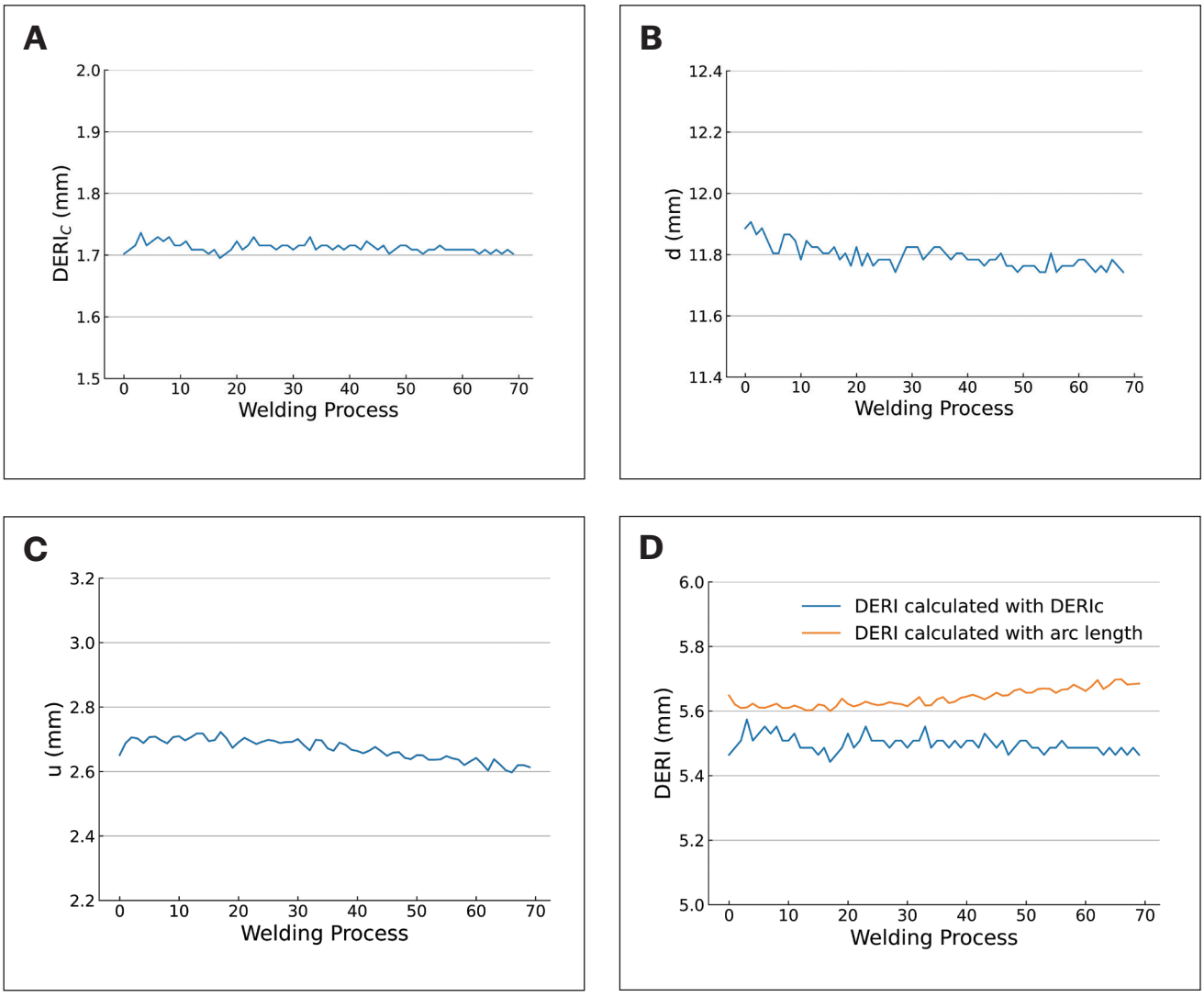

Fig. 7 — Curves obtained in experiment I: A — $DERI_C$ vs. welding process; B — d vs. welding process; C — u vs. welding process; D — DERI calculated with two methods.

parameter. The range and increasing trend of the curves imply that the X-axis and Y-axis deflection models are correct.

In Experiment V, the curve of the arc length agrees well with the offset distance of the welding torch during the welding process. The result suggests that the Z-axis offset model is correct and the established linear relationship between voltage and arc length is accurate.

In each experiment, based on the highly robust image processing algorithm and the high-precision linear relationship between welding voltage and arc length, the calculation errors of the required parameters in the REI-TPA model were small. When calculating the offset distance and deflection angle of the welding torch, the error increased due to the overlapping error of each required parameter and the amplification effect of an inverse trigonometric function. This error can be reduced by improving the accuracy of the experimental equipment. In addition, it is difficult to extract the position of the weld seam in the passive vision weld pool image. Thus, it is difficult to calculate the offset distance of the welding torch along the X-axis. This problem can be solved by adding active light sources or additional cameras.

Compared with these shortcomings, the REI-TPA model has more significant advantages: (1) The required information of the model was extracted from the passive vision image of the weld pool. Without additional sensors or active light sources, the experiment setup is simple and low-cost. (2) The position and attitude of the welding torch were directly calculated from the weld pool image of the welding point; almost no lag exists. (3) The model can be applied to the real-time monitoring of TPA by improving the accuracy of the sensors. (4) Combined with multi-information fusion technology, the REI-TPA model can be applied to predict numerous factors affecting the weld quality simultaneously, such as the weld penetration state, quality of the produced weld, and position and attitude of the welding torch. The REI-TPA model is a supplement to and extension of the acquisition and application of weld passive vision sensing technology.

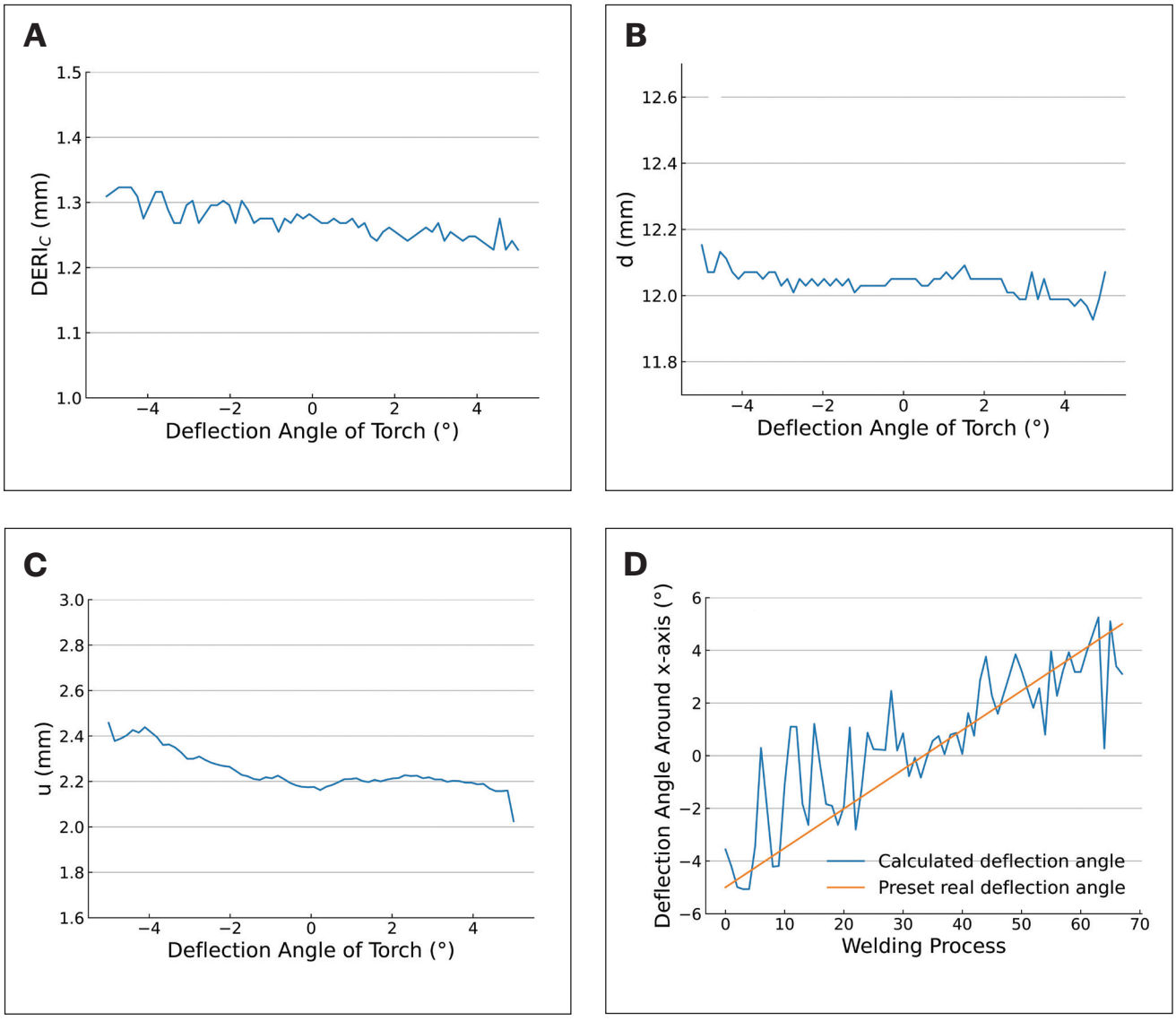

Fig. 8 — Curves obtained in experiment III: A — $DERI_c$ vs. deflection angle; B — d vs. deflection angle; C — u vs. deflection angle; D — Calculated deflection angle of welding torch around the X-axis.

Quality of the Obtained Images

The main factors influencing imaging quality include the quality of the camera, the intensity of the welding current, and the generation of the oxides.

To ensure the contrast between foreground and background in the image, a large dynamic range of the image captured by the camera is required. In addition, to guarantee the computational accuracy of the REI-TPA model, a high-resolution camera is required. For reference, in this research, the dynamic range of the image captured by the camera was more than 140 dB and the resolution of the camera was 1280 × 1024 pixels.

Low levels of current (100 A, 120 A) were applied in the experiment to ensure the relative stability of the weld pool. In this case, the arc radiation was weak. In addition, a dimmer was set in front of the camera lens to prevent the arc light from covering the REI and electrode in the image. The aperture was set at f.22 to reduce the amount of light reaching the image sensor.

During the welding process, few oxides were generated. Most of the oxides moved toward the edge of the weld pool due to the influence of arc pressure and gravity. In a few images, the oxides stayed in the central area of the weld pool, showing small, black holes in the binary image. The holes would be eliminated after morphological processing. In short, the oxides had little influence on image acquisition and feature extraction.

Conclusions

In the previous investigation (Ref. 1), the REI-TPA model was established to calculate the position and attitude of the

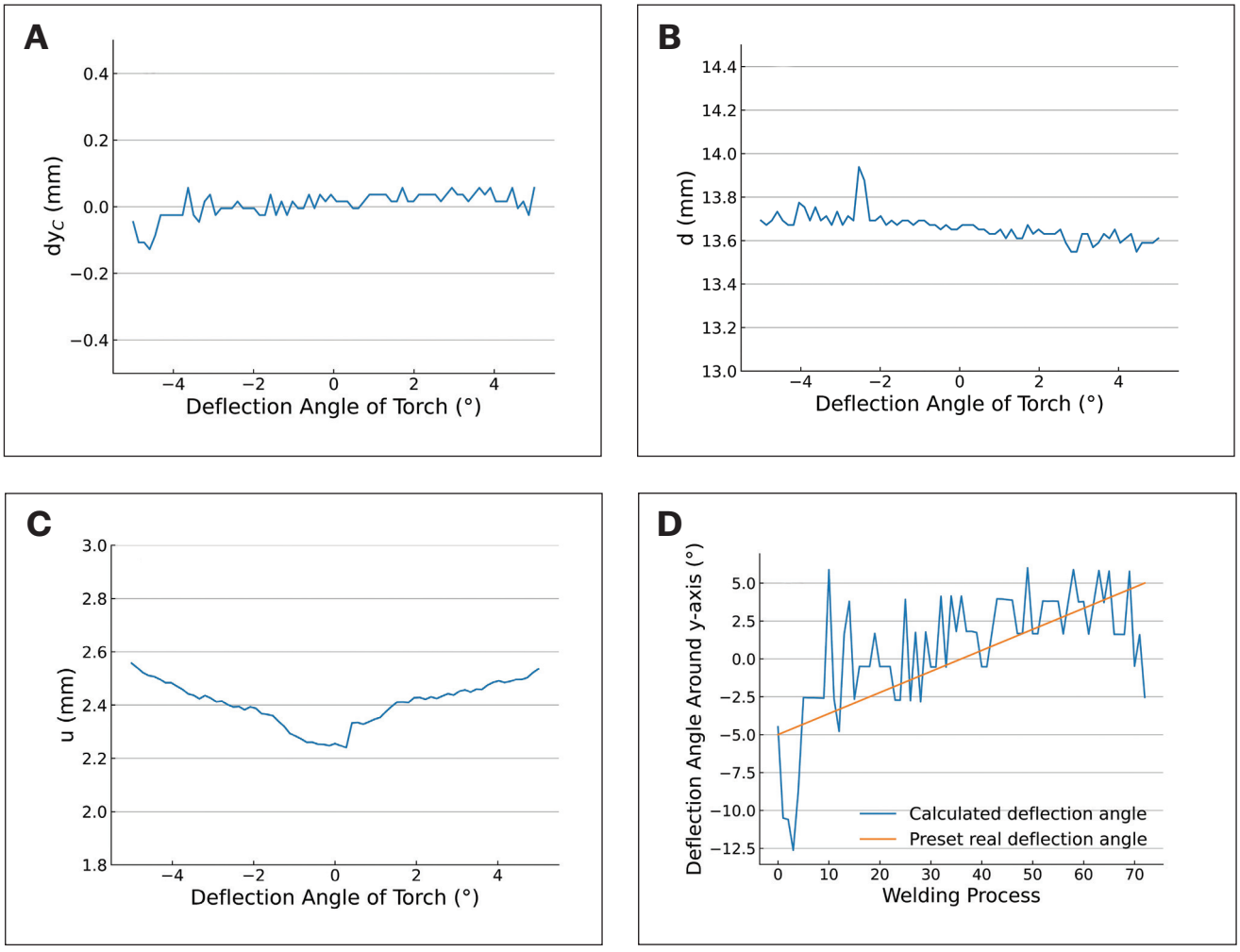

Fig. 9 — Curves obtained in experiment IV: A — dy_c vs. deflection angle; B — d vs. deflection angle; C — u vs. deflection angle; D — Calculated deflection angle of welding torch around the Y-axis.

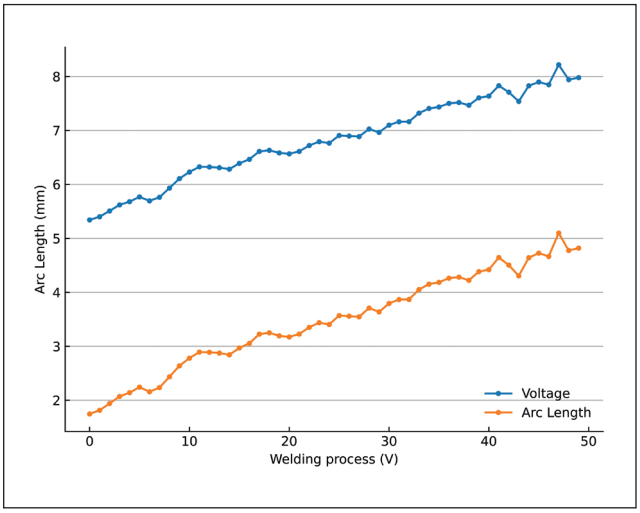

Fig. 10 — Welding voltage and calculated arc length in Experiment V.

welding torch in real time. In this research, the REI-TPA model was validated with bead-on-plate welding experiments on S304 stainless steel plates. The required parameters were extracted and calculated with a developed robust algorithm. The offset distance and deflection angle of the welding torch relative to the correct position and attitude were calculated and compared to the preset data. The result shows that the model is correct and the monitoring of a welding torch with the REI-TPA model is possible.

The REI-TPA model is of significance to automated welding and weld quality control, which is a supplement to weld visual sensing technology and an expansion to the acquisition and processing of multi-source information during the welding process.

In future research, the real-time monitoring and correction of TPA with the REI-TPA model, the extended application of the REI-TPA model, and the development of algorithms in seam tracking during the robotic welding process will be investigated.

Acknowledgments

This work is partly supported by the National Natural Science Foundation of China under Grant No. 61873164.

References

1. Fu, Y., Chen, Z., and Chen S. Monitoring welding torch position and posture using reversed electrode images — Part I establishment of the REI-TPA model. *Welding Journal* 103(7): 215-s to 223-s.

2. Zhang, Y., Wang, Q., and Liu, Y. 2021. Adaptive intelligent welding manufacturing. *Welding Journal* 100(1): 63–83.

3. Chen, S., and Lv, N. 2014. Research evolution on intelligentized technologies for arc welding process. *Journal of Manufacturing Processes* 16(1): 109–122.

4. Chen, Z., Feng, Z., and Chen, J. 2020. *Key technologies of intelligentized welding manufacturing: visual sensing of weld pool dynamic characters and defect prediction of GTAW process*. Springer.

5. Zhang, G., Shi, Y., Gu, Y., et al. 2017. Welding torch attitude-based study of human welder interactive behavior with weld pool in GTAW. *Robotics and Computer-Integrated Manufacturing* 48: 145–156.

6. Chen, Z., Chen, J., and Feng, Z. 2017. Monitoring weld pool surface and penetration using reversed electrode images. *Welding Journal* 96(10).

7. Chen, Z., Chen, J., and Feng, Z. 2019. 3D Weld pool surface geometry measurement with adaptive passive vision images. *Welding Journal* 98(12): 379-s to 386-s.

8. Chen, Z., Chen, J., and Feng, Z. 2018. Welding penetration prediction with passive vision system. *Journal of Manufacturing Processes* 36: 224–230.

9. Feng, Y., Chen, Z., Wang, D., et al. 2019. DeepWelding: A deep learning enhanced approach to GTAW using multisource sensing images. *IEEE Transactions on Industrial Informatics* 16(1): 465–474

10. Xu, Y., Fang, G., Lv, N., et al. 2015. Computer vision technology for seam tracking in robotic GTAW and GMAW. *Robotics and Computer-Integrated Manufacturing* 32: 25–36.

11. Xu, Y., Yu, H., Zhong, J., et al. 2012. Real-time seam tracking control technology during welding robot GTAW process based on passive vision sensor. *Journal of Materials Processing Technology* 212(8): 1654–1662.

12. Chen, S., Lou, Y., Wu, L., and Zhao, D. 2000. Intelligent methodology for sensing, modeling and control of pulsed GTAW: Part 1 — Bead-on-plate welding. *Welding Journal* 79(6): 51-s to 163-s.

13. Chen, S., et al. 2000. Intelligent methodology for sensing, modeling and control of pulsed GTAW: Part 2 — Butt joint welding. *Welding Journal* 79(6): 164-s to 174-s.

14. Wu, J., and Chen, S. 2007. Software system designs of real-time image processing of weld pool dynamic characteristics. *Robotic Welding, Intelligence and Automation*: 303–309.

15. Xiao, R., Xu, Y., Hou, Z., et al. 2021. An automatic calibration algorithm for laser vision sensor in robotic autonomous welding system. *Journal of Intelligent Manufacturing* 1–14.

16. Xiao, R., Xu, Y., Hou, Z., et al. 2021. A feature extraction algorithm based on improved Snake model for multi-pass seam tracking in robotic arc welding. *Journal of Manufacturing Processes* 72: 48–60.

17. Kovacevic, R., Zhang, Y., and Ruan, S. 1995. Sensing and control of weld pool geometry for automated GTA welding. *Journal of Engineering for Industry* 117(2): 210-222.

18. Zhang, Y., Kovacevic, R., and Li, L. 1996. Characterization and real-time measurement of geometrical appearance of the weld pool. *International Journal of Machine Tools and Manufacture* 36(7): 799–816.

19. Zhang, Y., and Kovacevic, R. 1998. Neurofuzzy model-based predictive control of weld fusion zone geometry. *IEEE Transactions on Fuzzy Systems* 6(3): 389–401.

20. Song, H., and Zhang, Y. 2008. Measurement and analysis of three-dimensional specular gas tungsten arc weld pool surface. *Welding Journal* 87(4): 85-s to 95-s.

21. Wang, Z., Zhang, Y., and Yang, R. 2013. Analytical reconstruction of three-dimensional weld pool surface in GTAW. *Journal of Manufacturing Processes* 15(1): 34–40.

22. Zhang, Z. 2000. A flexible new technique for camera calibration. *IEEE Transactions on pattern analysis and machine intelligence* 22(11): 1330–1334.

23. Chen, Z., Chen, J., and Feng, Z. 2017. Monitoring weld pool surface and penetration using reversed electrode images. *Welding Journal* 96(10).

24. Dos, Santos., E, B., et al. 2017. On the visualization of gas metal arc welding plasma and the relationship between arc length and voltage. *Applied Sciences* 7(5): 503.

25. Li, P., and Zhang, Y. 2001. Robust sensing of arc length. *IEEE Transactions on Instrumentation and Measurement* 50(3): 697–704.

26. Muhammad, J., and Altun, H., Abo-Serie, E. 2017. Welding seam profiling techniques based on active vision sensing for intelligent robotic welding. *The International Journal of Advanced Manufacturing Technology* 88(1): 127–145.

27. Ushio, M., and Mao, W. 1994. Sensors for arc welding advantages and limitations. *Transactions of JWRI* 23(2): 135–141.

28. Bae, K., Lee, T., and Ahn, K. 2002. An optical sensing system for seam tracking and weld pool control in gas metal arc welding of steel pipe. *Journal of Materials Processing Technology* 120(1-3): 458–465.

29. Huang, W., and Kovacevic, R. 2012. Development of a real-time laser-based machine vision system to monitor and control welding processes. *The International Journal of Advanced Manufacturing Technology* 63(1): 235–248.

YU FU, **QIANG LIU**, **RUNQUAN XIAO**, and **SHANBEN CHEN** (*sbchen@sjtu.edu.cn*) are with Shanghai Jiao Tong University, Shanghai, People's Republic of China.